

## Supporting information

### Theoretical and experimental studies on three water-stable, isostructural, paddlewheel based semiconducting metal-organic frameworks

Xiaowei Yang,<sup>a†</sup> Yuan Zhang,<sup>b†</sup> Feng Li,<sup>a</sup> Tiantian Guo,<sup>a</sup> Yong Wu,<sup>a</sup> Fengyan Jin,<sup>a</sup> Min Fang,<sup>\*acd</sup> Yaqian Lan,<sup>a</sup> Yafei Li<sup>\*a</sup>, Yong Zhou,<sup>\*b</sup> Zhigang Zou<sup>b</sup>

- a. Department of Chemistry, School of Chemistry and Materials Science, Nanjing Normal University, Nanjing 210023, China. Email: fangmin@njnu.edu.cn, liyafei@njnu.edu.cn
- b. Ecomaterials and Renewable Energy Research Center (ERERC), Nanjing University, 22 Hankou Road, Nanjing, Jiangsu 210093, P. R. China. Email: zhouyong1999@nju.edu.cn
- c. State Key Laboratory of Coordination Chemistry, Nanjing University, Nanjing 210093, China.
- d. Jiangsu Key Laboratory for Numerical Simulation of Large Scale Complex Systems (NSLSCS), Nanjing Normal University, Nanjing 210023, China

\* Corresponding authors.

† These authors contribute equally to this paper.

**Keywords:** DFT calculation, band structure, band gap, visible light, CO<sub>2</sub> reduction, methane

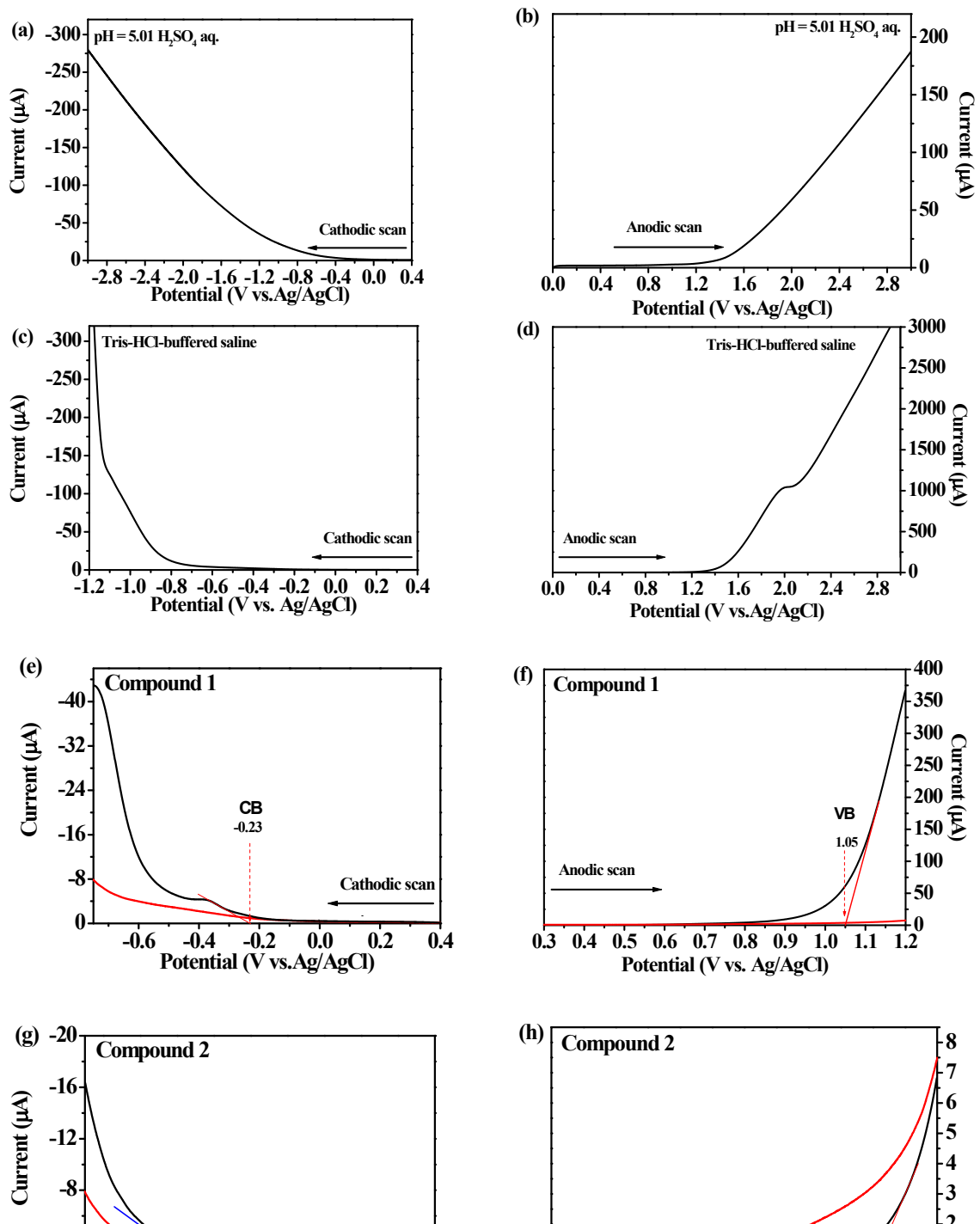
## Contents

<b>Determination of conduction and valence band edges by the electrochemical method .....</b>	3
<b>Fig. S1</b> Cathodic and anodic linear potential scan for determining the positions of the conduction band (CB) and valence band (VB) edges of MOFs <b>1-3</b> specimens at 100 mV/s.....	4
<b>Tentative assignments of IR and Raman spectra of MOFs <b>1-4</b>.....</b>	4
<b>Fig. S2</b> IR and Raman spectra of MOFs <b>1-4</b> compared with that of BPY in the range of 4000-400 cm <sup>-1</sup> ....	6
<b>Fig. S3</b> IR and Raman spectra of MOF <b>3</b> compared with spectra of related paddlewheel MOFs (2000-200 cm <sup>-1</sup> ). ....	7
<b>Fig. S4</b> IR and Raman spectra of MOF <b>3</b> compared with spectra of related MOFs in the range of 4000-400 cm <sup>-1</sup> . ....	8
<b>Table S1</b> Tentative assignments for the IR and Raman spectra of <b>1-4</b> .....	9
<b>Synthesis of MOF 1 in DMF .....</b>	10
<b>Synthesis of MOF 3 in DMA and NMP mixed solvent .....</b>	10
<b>Fig. S5</b> The powder X-ray diffraction (PXRD) patterns of the products of large scale preparations of MOF <b>1(a)</b> , <b>2(b)</b> and <b>3(c)</b> .....	10
<b>Fig. S6</b> PXRD patterns of MOFs <b>1(a)</b> , <b>2(b)</b> and <b>3(c)</b> synthesized in various solvent systems. ....	11
<b>Table S2</b> Crystallographic data for MOFs <b>1-3</b> and <b>5</b> .....	12
<b>Table S3</b> Selected bond distances and angles MOF <b>1-3</b> .....	13
<b>Table S4</b> Pore sizes (Å) and porosities of MOFs <b>1-3</b> .....	13
<b>Fig. S7</b> The asymmetric units of MOFs <b>1 (a)</b> , <b>2 (b)</b> and <b>3 (c)</b> .....	14
<b>Fig. S8</b> The 3D packing of MOFs <b>1</b> and <b>2</b> , viewing along <i>b</i> and <i>c</i> axes.....	14
<b>Fig. S9</b> PXRD of MOFs <b>1-3</b> heated at various temperatures for 12 h. ....	15
<b>Fig. S10</b> Thermal stability of MOFs <b>1- 3</b> checked by IR spectra.....	16
<b>Fig. S11</b> Nitrogen gas sorption isotherms for MOFs <b>1-3</b> measured at 77 K. ....	16
<b>Fig. S12</b> The H <sub>2</sub> sorption isotherms for MOFs <b>1-3</b> measured at 77 K and N <sub>2</sub> , CH <sub>4</sub> and CO <sub>2</sub> sorption isotherms for MOFs <b>1-3</b> measured at 298 and 273 K. ....	17
<b>Fig. S13</b> CO <sub>2</sub> sorption isotherms of compound <b>3</b> (recovered after 24 h in water) at 298 K.....	17
<b>Fig. S14</b> UV-Vis spectra (R% versus Wavelength) of H <sub>4</sub> TCS, BPY and MOFs <b>1-3</b> . ....	18
<b>Table S5</b> The total energies of the optimized structures of the unit cells of MOFs <b>1-3</b> using the GGA-PBE method.....	18
<b>Table S6</b> Valence and conduction band edges and band gaps of MOF <b>1</b> and <b>3</b> calculated by GGA-PBE and different GGA-PBE + U methods. ....	18
<b>Table S7</b> Valence and conduction band edges and band gaps of MOF <b>2</b> calculated by GGA-PBE and different GGA-PBE + U methods. ....	19
<b>Fig. S15</b> Enlarged band structures (GGA-PBE method) of the spin-up and spin-down electrons of MOF <b>1</b> , showing MOF <b>1</b> is an indirect band gap semiconductor. ....	19
<b>Fig. S16</b> Enlarged band structures (GGA-PBE + U (U=3.3) method) of the spin-up and spin-down electrons of MOF <b>2</b> , showing it is an indirect band gap semiconductor.....	19
<b>Fig. S17</b> Enlarged band structures (GGA-PBE + U (U = 4.0) method) of the spin-up and spin-down electrons of MOF <b>3</b> , showing it is an indirect band gap semiconductor.....	20
<b>Fig. S18</b> Raman Spectrum of the liquid N,N-dimethylformamide.....	20
<b>References .....</b>	20

## Determination of conduction and valence band edges by the electrochemical method

This study subjected the conduction band edge (LUMO) and valence band edge (HOMO) positions of MOFs **1-3** to analysis with linear potential scans according to the method given in the literature.<sup>1-2</sup>

Different from the literature, we used two kinds of electrolytes, the Tris-HCl-buffered saline ( $0.1 \text{ mol L}^{-1}$ , pH 7.4) and a pH 5.01  $\text{H}_2\text{SO}_4$  aqueous solution. The current versus potential of both electrolytes with the same scanning rate were recorded by using the ITO electrodes which were not modified by compounds so that the shape of the current curves due to the electrolytes might be known (Fig. S1a-d) and the sharp increases of currents due to the redox reactions of the electrolytes would not be treated as band edges of compounds in the following measurements. It is found that the Tris-HCl-buffered saline ( $0.1 \text{ mol L}^{-1}$ , pH 7.4) is suitable to study band edges in the range of -0.7-1.4 eV, and the a pH 5.01  $\text{H}_2\text{SO}_4$  aqueous solution is suitable to study band edges in the range of -0.4-1.2 eV since no obvious current are observed in these ranges. If the background current is large, the determined absolute values of the band edges would have a positive deviation. When determining the band edges, the current curves due to MOFs were compared with the current curves (in red) of the electrolytes. We did not deduct the current of the red curves in determining the band edges since the red curves are obtained when the ITO electrodes are not modified with MOFs. And after the modification, the current density due to the electrolytes become smaller due to the different conductivity of the modified ITO electrode. We found it is hard to tell the band edges of MOFs **1-3** when using the pH 5.01  $\text{H}_2\text{SO}_4$  aqueous solution as the electrolyte. However, it clearly gave the conduction band edge position of MOF **3**, which is exactly the same as that determined using the Tris-HCl-buffered saline solution. The band edge positions of MOF **1-3** are shown in Fig. S1e-k and are summarized in Table 2.



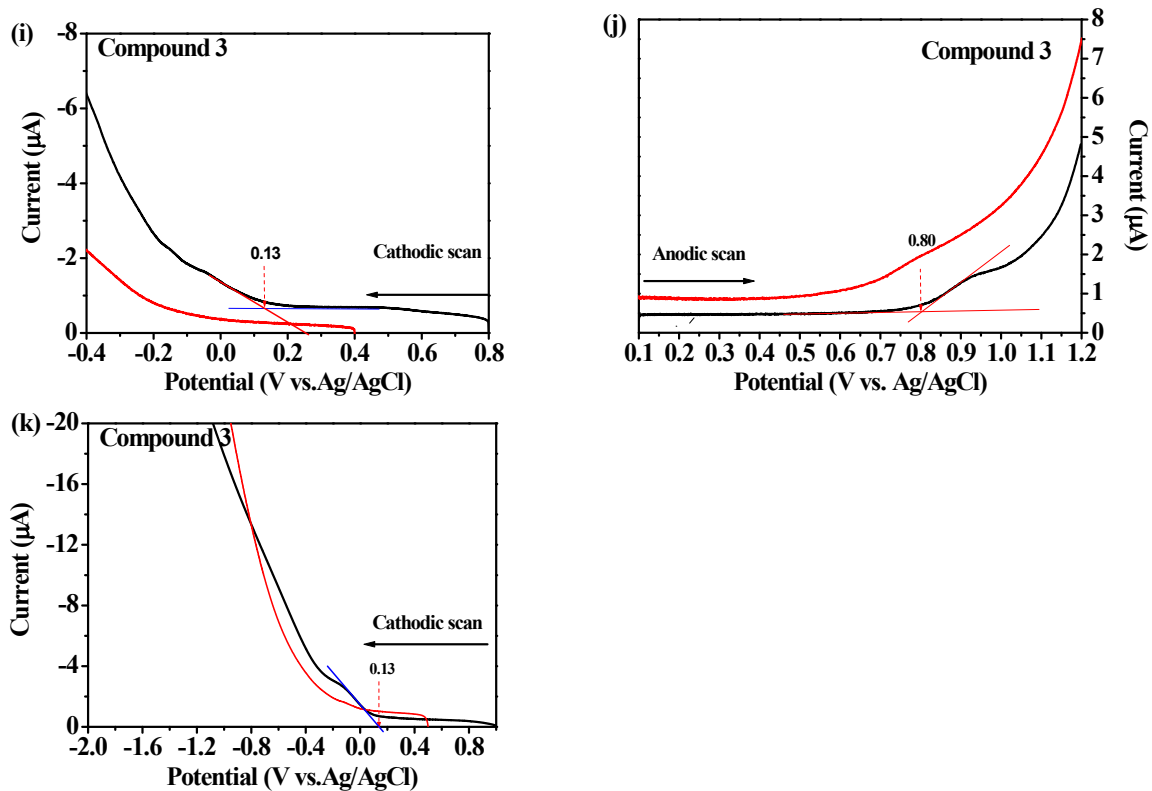


**Fig. S1** Cathodic and anodic linear potential scan for determining the positions of the conduction band (CB) and valence band (VB) edges of MOFs **1** (e-f), **2** (g-h) and **3** (i-k) specimens at 100 mV/s. The current to potential curves of the electrolytes with the same scanning rate using unmodified ITO electrodes are shown in (a)-(d). (e)-(j) were obtained using the Tris-HCl buffered saline solution, and (k) was obtained using the pH = 5.01 H<sub>2</sub>SO<sub>4</sub> aqueous solution. The red curves are the currents of the electrolytes obtained using the unmodified ITO electrodes, same as those in (a)-(d).

### Tentative assignments of IR and Raman spectra of MOFs 1-4

The IR and Raman spectra of **1-4** (Fig. 3) are very similar to each other; the tentative assignments of the vibrational frequencies are given in Table S1. MOFs **1-4** contains both BPY and TCS<sup>4-</sup> ligands. The IR and Raman spectra of BPY and Co(II), Ni(II) and Zn(II) complexes of BPY have been assigned by Bing *et al.*<sup>3</sup> and Topaçlı *et al.*<sup>4</sup> Based on their results we are able to assign the BPY related vibration modes. Wang *et al.*<sup>5</sup> assigned some IR frequencies of H<sub>4</sub>TCS: 3025 (arom. C-H), 2552 (-COOH), 1694 (-C=O, carboxyl), 1498 (arom. C=C), 759 (Si-C), 708 (arom. p-subst.). We measured the IR and Raman spectra of H<sub>4</sub>TCS and compared them with those of MOF **3** in Fig. S3 and S4. In order to assign the M-O, M-N, M-M and COO<sup>-</sup> vibrational frequencies, we also compared the spectra of **1-3** with IR and Raman spectra of Cu<sub>3</sub>(BTC)<sub>2</sub> (BTC = benzene-1-3-5-tricarboxylate),<sup>6,7,8</sup> the IR spectra of paddlewheel based Cu<sub>2</sub>(TCS)<sub>2</sub>(H<sub>2</sub>O)<sub>2</sub> (PCN-512) reported by Zhou *et al.*,<sup>9</sup> and also the IR and Raman frequencies of M(BDC)(TED)<sub>0.5</sub> (M = Cu(II), Zn(II), Ni(II), Co(II); BDC = 1,4-benzenedicarboxylate; TED = triethylenediamine) assigned by Chabal *et al.*<sup>10</sup> Weak bands in the range of 2000-1650 cm<sup>-1</sup>

in the IR spectra of MOFs **1-4** were assigned as combination bands, the pattern of which is consistent with the para-disubstituted benzene rings.<sup>11</sup>

**CO<sub>2</sub><sup>-</sup> bond vibrations** The carboxylate symmetric stretch of Cu<sub>3</sub>(BTC)<sub>2</sub> is assigned as two bands at 1450 (m) and 1375 cm<sup>-1</sup> (s), while the asymmetric stretch is observed at 1650 (m) and 1419 cm<sup>-1</sup> (w).<sup>6</sup> 1112 and 938 cm<sup>-1</sup> are assigned to the C–H in-plane and out-of-plane bending modes respectively, while the bands at 757 and 729 cm<sup>-1</sup> coincide with the C–C ring out-of-plane bending modes.<sup>8</sup> The most notable changes in the spectra occur with the gradual appearance of bands at 1708 and 1243 cm<sup>-1</sup> corresponding to the C=O and C–O stretching bands of a carboxylic acid when it was subject in high humidity environment.<sup>8</sup> The frequency difference of symmetric and asymmetric stretch of carboxylate with bridging bidentate configuration (the paddle wheel structure belongs to this type) gives values in the range of 160–200 cm<sup>-1</sup>.<sup>12</sup> Based on this regularity and the IR intensity of  $\nu_{\text{sym}}(\text{COO})$  is weaker than the IR intensity of  $\nu_{\text{asym}}(\text{COO})$ , Chabal *et al.*<sup>10</sup> assigned the bands at 1622 and 1430 cm<sup>-1</sup> of the IR spectrum of [Cu<sub>2</sub>(BDC)<sub>2</sub>(TED)]· to the  $\nu_{\text{asym}}(\text{COO})$  and  $\nu_{\text{sym}}(\text{COO})$  modes. The band at 1703 cm<sup>-1</sup> (IR) of MOF **3** increases and the band at 1611 cm<sup>-1</sup> decreases as shown in Fig. S10 when the sample was heated at 200 °C for 12 h. And we know MOF **3** decomposes after repeated heating (each time at 150 °C under vacuum for 10 h). We therefore deduce that the band at 1703 cm<sup>-1</sup> is due to the C=O of COOH groups which was formed during the heating process and the band at 1611 is due to the  $\nu_{\text{asym}}(\text{COO})$  of MOF **3**. A medium strong band at 1703 cm<sup>-1</sup> appears in the Raman spectrum of as-synthesized MOF **3**, which are not shown in Raman spectra of MOFs **1-2**. The Raman of H<sub>4</sub>TCS only shows a very weak band at 1690 cm<sup>-1</sup>, indicating that  $\nu_{\text{asym}}(\text{C=O})$  of COOH is not obvious in Raman spectrum. Thus, the band at 1703 cm<sup>-1</sup> in the Raman spectrum of MOF **3** is assigned as a combination band of benzene ring. The weak band in the range of 1703–1719 cm<sup>-1</sup> of the IR spectra of as-synthesized MOFs **1-4** was assigned as a combination band of benzene ring, consistent with the pattern of para-disubstituted benzene ring.<sup>11</sup> Based on these results and other related results,<sup>13-14</sup> we assigned the IR bands at 1611 and 1420 cm<sup>-1</sup> of MOF **3** to the  $\nu_{\text{asym}}(\text{COO})$  and  $\nu_{\text{sym}}(\text{COO})$  modes, respectively and also assigned the related IR and Raman bands for MOFs **1, 2** and **4**.

**M-N and M-O bond vibrations** Nakamoto *et al.* localized the M-N bond stretching vibrations in the far-infrared spectra of metal complexes with 2,2'-BPY ligand.<sup>15</sup> They are 266 and 228 cm<sup>-1</sup> for Co(II), 282 and 258 cm<sup>-1</sup> for Ni(II), 291 and 268 cm<sup>-1</sup> for Cu(II), 230 and 184 cm<sup>-1</sup> for Zn(II). Drozdzewski *et al.*<sup>16</sup> localized metal–ligand vibrations in the far-infrared spectrum of polymeric [ZnCl(IA)(HIA)]H<sub>2</sub>O complex (HIA denotes the 4-imidazoleacetic acid) with the help of metal isotope, Cl–Br substitution effects and the density functional theory calculations. Band at 494 cm<sup>-1</sup> is attributed to  $\delta(\text{OCC})$  and  $\nu(\text{Zn–O})$  (Zn–O bond distances: 1.979(2) and 1.981(2) Å) with the energy contribution of  $\nu(\text{Zn–O})$  less than one-third and the band at 245 cm<sup>-1</sup> is attributed to  $\nu(\text{Zn–N})$  (Zn–N bond distance: 1.987(2) Å). Morzyk-Ociepa *et al.* assigned the IR band at 495 cm<sup>-1</sup> (m) of the paddlewheel based diamminetetrakis-m- (O,O'-indole-3-carboxylate)dicopper(II) to Cu–O stretching vibration (bond distance: 1.961(2) and 1.970(2) Å) based on the theoretical calculation result. Jim *et al.*<sup>6</sup> assigned the two bands at 505 (strong) and 449 cm<sup>-1</sup> (weak) and a doublet in the 193–172 cm<sup>-1</sup> range in the Raman spectrum of Cu<sub>3</sub>(BTC)<sub>2</sub> (Cu-HKUST) to Cu–O and Cu–Cu stretching modes, respectively. Navrotsky *et al.*<sup>17</sup> assigned 455 cm<sup>-1</sup> (s) in the IR spectrum to the Zn–O stretching mode (2.025(2) Å) of Zn-HKUST. Little change in the Zn–O band was seen after chloroform exchange. Upon thermal activation the Zn–O vibration split into three distinct bands (450, 463, and 477 cm<sup>-1</sup>), indicating a change in the initial symmetry likely due to deformation of the paddle wheel structure. The IR band at 489 cm<sup>-1</sup> (m) of Cu-HKUST (spectrum given in ref 18 could be assigned to the Cu–O stretching frequency (1.952(4) Å). Based on the above results, we assigned the IR bands from 479–500 cm<sup>-1</sup> to M–O stretching modes; the weak bands at 296 cm<sup>-1</sup> in the Raman spectrum of MOF **1**, at 306 cm<sup>-1</sup> in the Raman spectrum of MOF **2** and at 284 and 274 cm<sup>-1</sup> in the Raman spectrum of MOF **3** were assigned to the M–N stretching modes.

**M-M bond vibrations** Jim *et al.*<sup>6</sup> assigned the doublet in the 193–172 cm<sup>-1</sup> range of the Raman spectrum of Cu<sub>3</sub>(BTC)<sub>2</sub> to Cu–Cu stretching modes. We assigned the Raman bands at 217 and 219 cm<sup>-1</sup> to Co–Co and Ni–Ni stretching modes. Cu–Cu stretching were not observed, this mode is probably below 200 cm<sup>-1</sup>.

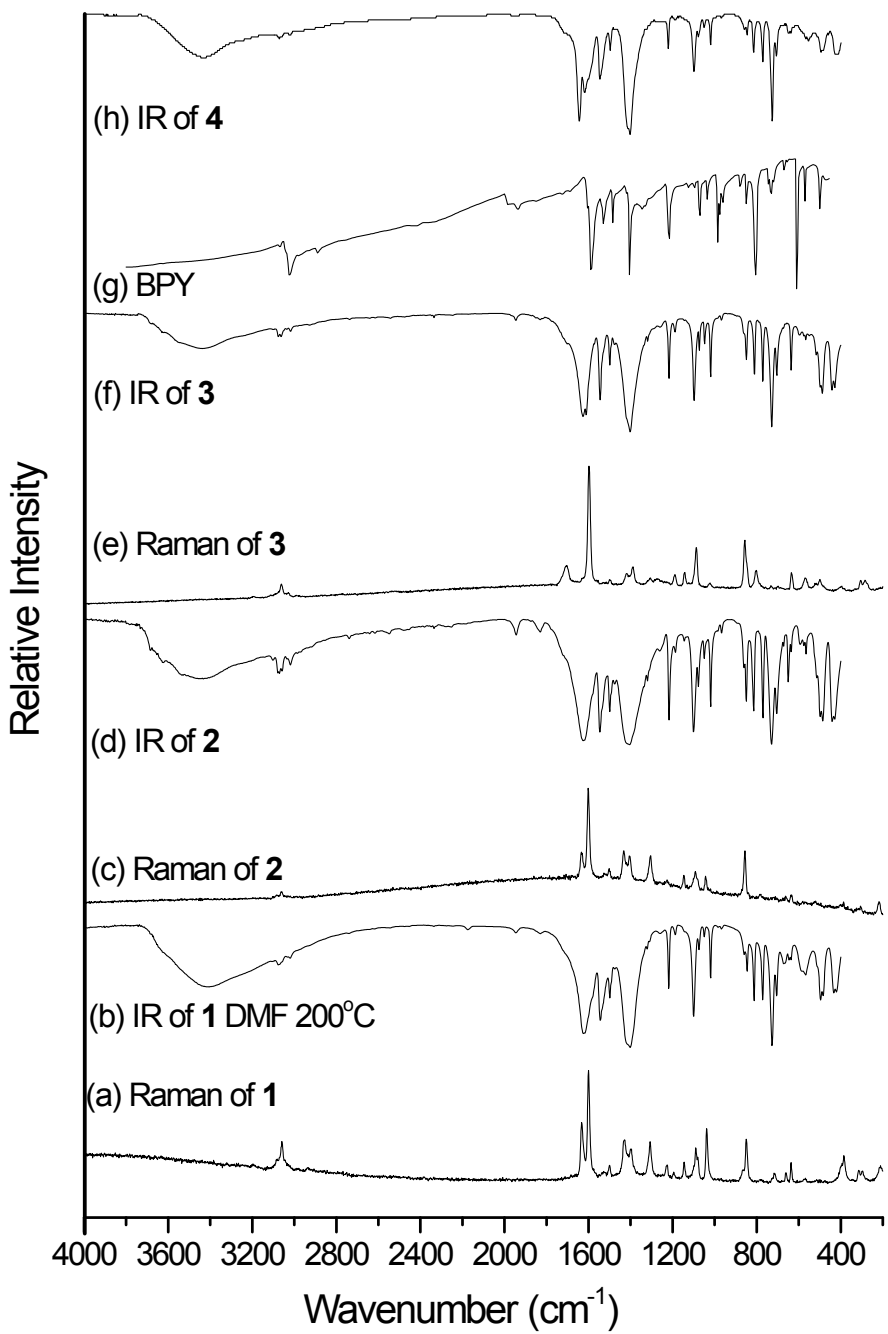


**Fig. S2** IR and Raman spectra of MOFs **1-4** compared with that of BPY in the range of 4000-400  $\text{cm}^{-1}$ .

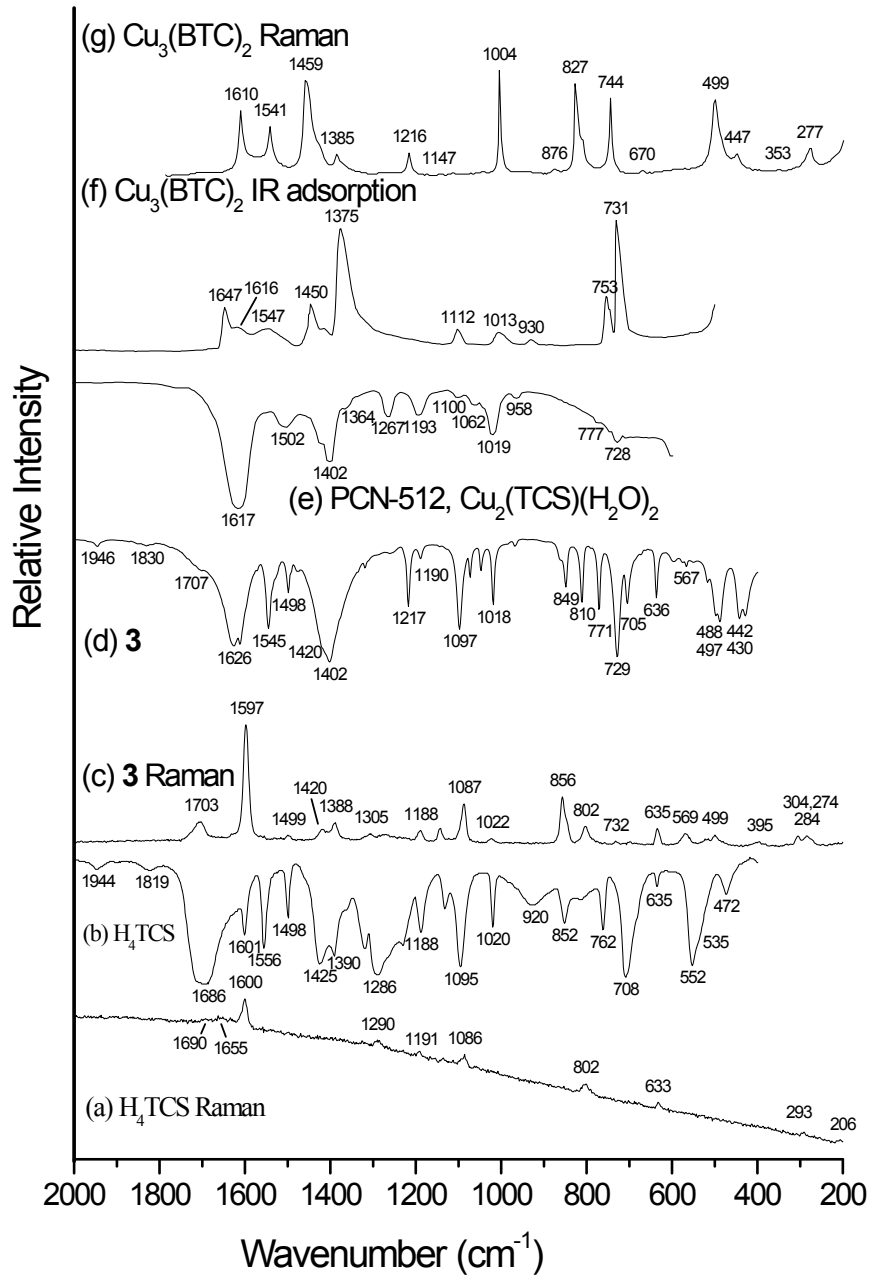


**Fig. S3** IR and Raman spectra of MOF **3** compared with spectra of related paddlewheel MOFs (2000–200 cm<sup>-1</sup>).

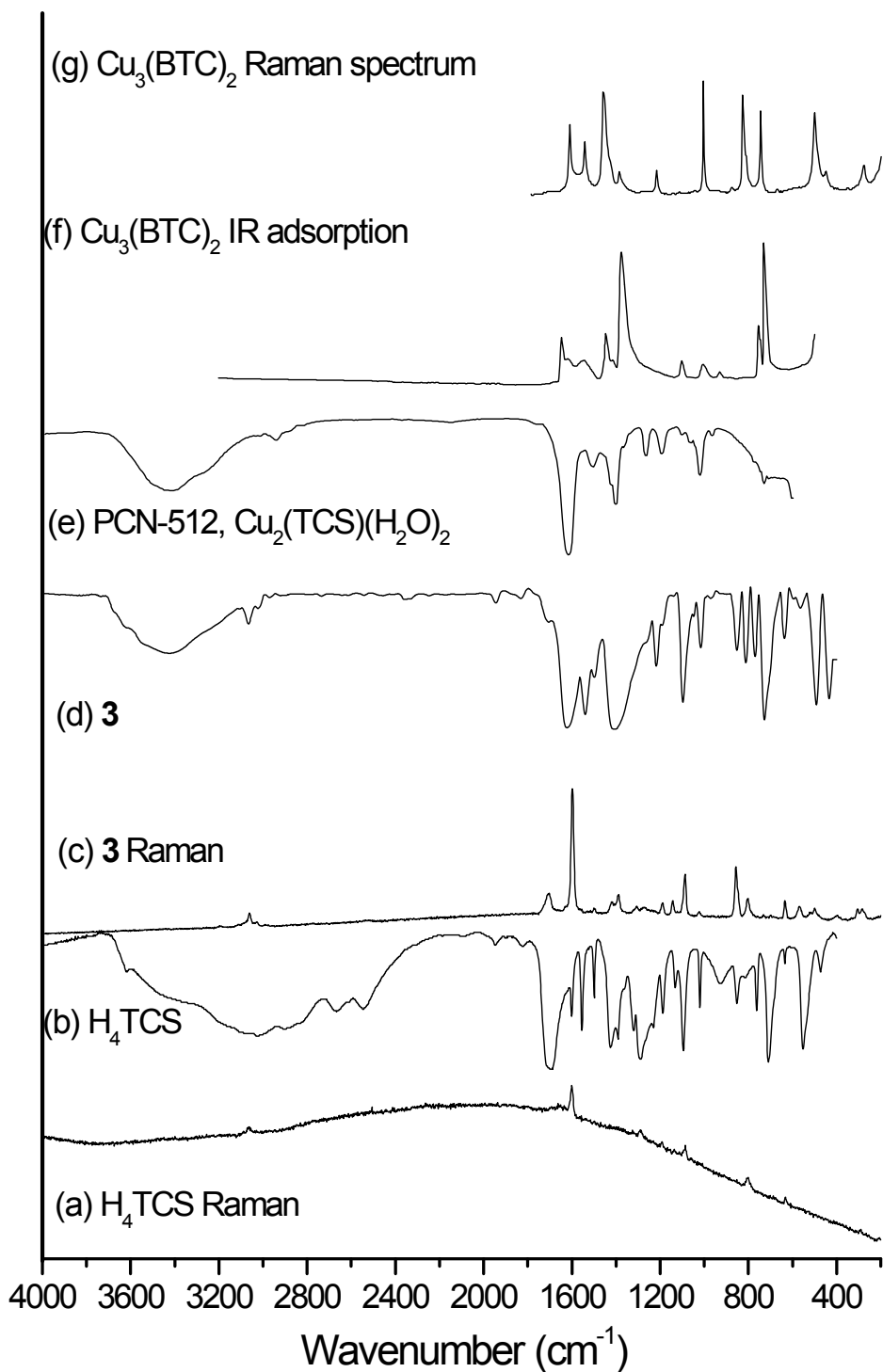


Fig. S4 IR and Raman spectra of MOF **3** compared with spectra of related MOFs in the range of 4000-400 cm<sup>-1</sup>.

**Table S1** Tentative assignments for the IR and Raman spectra of **1-4**.

<b>1</b> (IR)	<b>1</b> (Raman)	<b>2</b> (IR)	<b>2</b> (Raman)	<b>3</b> (IR)	<b>3</b> (Raman)	<b>4</b> (IR) <sup>a</sup>	Tentative assignment
3435 b		3432b		3407 b		3442 b	H <sub>2</sub> O
3076 w	3074 vw	3076 w	3083 vw	3104 w	3076 w	3070 w	u(C-H) of benzene u(C-H)
3020 w	3060 w	3062 w	3063 w	3070 w	3062 w	3019 w	BPY ring
		3035 vw		3060 w	3035 vw		
		3019 w		3033 vw			
				3018 w			
2736 vw		2738 vw		2736 vw		2444 vw	
2549 vw		2546 vw		2544 vw		2334 vw	
2455 vw		2464 vw		2455 vw			
2335 vw		2332vw		2335vw			
2248 vw		2266 vw		2245 vw			
2173 w							
1946 w		1946 w		1946 vw		1936 vw	
1830 w		1830 w		1830 vw		1851 vw	
-		1780 vw		1780 vw		1774 vw	
1719 w	-	1707 w		1703 w	1703 m	1716 w	Combination band
1624 s	1633m	1626 s	1634m	1626 s		1643 s	u(C=N)
1600 s		1611 s		1611 s	1629 vw	1618 s	u <sub>as</sub> (COO)
	1600 s		1602 s		1597 s	1599 s	u (C=C)
1580 sh		1580 sh		-			u benzene ring
1545 s		1545 s		1545 s		1545 s	u benzene ring
-	1528 vw	1529 w	1523 vw	1529 w	-		u(C=C), u(C=N)
1499 w	1500 w	1498 w	1502 w	1498 w	1499 w	1498 w	u benzene ring
1418sh	1429 m	1420 sh	1432 m	1420 sh	1420 m	1414 sh	u <sub>s</sub> (COO)
1402 s	1401m	1402 s	1407m	1402 s	1388m	1402 s	TCS Ring breathing
	1307 m		1304 m		1304 w		BPY Ring breathing, δ(C-H)
					1275 w		
1219 m	1226 w	1217 m	1226 w	1217 m	-	1221 m	δ(C-H) of BPY
1189 w	1195 vw	1190 w	1195 vw	1190 w	1188 w	1190 w	TCS
	1145 w		1146 w		1142 w		TCS
1099 s	1090 w	1097 s	1092 w	1097 s	1087 s	1099 m	TCS δ(C-H)
	1081 w		1078 w				
1076 w		1072 w		1072 w		1078 w	δ(C-H) of BPY
1048 w	1039 m	1050 w	1043 w	1048 w	1022 w	1048 w	BPY ring breathing+δ(C-H)
1018 m		1018 m		1018 m		1018 m	TCS ring breathing
968 w		968 w		968 w		966 vw	BPY ring breathing
860 w		863 w		863 w			γ(C-H) of BPY
	850 m		856 s		856 s		γ(C-H) of TCS
846 w		849 m		849 m		856 w	γ(C-H) of TCS
						845 w	
812 m		810 m		810 m	802 m	814 m	γ(C-H) of BPY
772 m		771 m	780 vw	771 m		771 m	u(Si-Ph)
727 s	718 w	729 s	718 w	729 s	732 vw	727 s	γ(C-H) of TCS
705 m		705 m		705 m	700 vw	704 m	γ(C-H) of TCS
671w		672 vw		670 vw			
662 vw		650 m	663 vw	636 m		647vw	δBPY ring <sup>4</sup>
643 vw							
638 vw	636 w	636 w	635 vw	636 m	635 m	636 vw	TCS
587 w		593 vw		596 w		590 vw	M-related
-	571 vw	577 vw		576 vw	569 m		BPY ring breathing

<b>1 (IR)</b>	<b>1 (Raman)</b>	<b>2 (IR)</b>	<b>2 (Raman)</b>	<b>3 (IR)</b>	<b>3 (Raman)</b>	<b>4 (IR)<sup>a</sup></b>	Tentative assignment
567 w		565 w		567 w		567 vw 552 vw	TCS
513 w		513 w	519 vw	515 w	519 vw	512 vw	$\gamma$ BPY ring <sup>4</sup>
496m		495m		497m	499 w	494 w	$\nu$ (M-O)
485 m		486 m		488 m		479 w	
434 m		442 m		442 m		428 w	M-related
420 m		428 m		430 m		413 w	M-related
		400 w	400 vw		395 w		$\delta$ BPY ring <sup>4</sup>
		385 m	387 vw				
		315 w	317 vw		304 w		$\delta$ BPY ring <sup>4</sup>
		296 w	306 vw		284 w 274 vw		$\nu$ (M-N)
		217 m	219 m		-		$\nu$ (M-M)

Abbreviations: m, medium; s, strong; sh, shoulder; w, weak, v, very; u, stretching; br, broad;  $\delta$ , in-plane bending;  $\gamma$ , out-of-plane bending; t, torsion; as, antisymmetric; s, symmetric; sciss, scissoring; rock, rocking; wag, wagging; twist, twisting; 5R, 5-membered indole ring; 6R, 6-membered indole ring. a. IR data of MOF 4 are from the SI of ref. <sup>19</sup>.

#### Synthesis of MOF 1 in DMF

$H_4TCS$  (6.4 mg, 0.0125 mmol), BPY (2.0 mg, 0.0125 mmol) and  $Co(NO_3)_2 \cdot 6H_2O$  (14.55 mg, 0.050 mmol) in 2.0 mL DMF were stirred for 10 min in a glass vial. The glass vial was then sealed in an autoclave equipped with a Teflon liner (25 mL) and put into an oven. The temperature of the oven was then raised to 150°C from room temperature, kept at 150 °C for 3 d, the heat was turned off, and the autoclave was cooled down to room temperature naturally in the oven, resulting in dark-blue powder. The powder was filtered and washed with DMF and then  $H_2O$ , dried at 60 °C for 12 h (yield: 8.0 mg, 80% based on  $H_4TCS$ ). Its purity was checked by PXRD (Fig. S6(a)).

#### Synthesis of MOF 3 in DMA and NMP mixed solvent

12.1 mg  $Cu(NO_3)_2 \cdot 3H_2O$  (0.050 mmol) was added, the reaction were carried out at 80 °C for 3 d, the solvent is a mixture of DMA (dimethylacetamide, 1 mL) and NMP (N-Methyl pyrrolidone, 1 mL), and other synthetic procedure are the same as in the preparation of MOF 1 in DMF. The purity of the product was checked by PXRD (Fig. S6(c)).

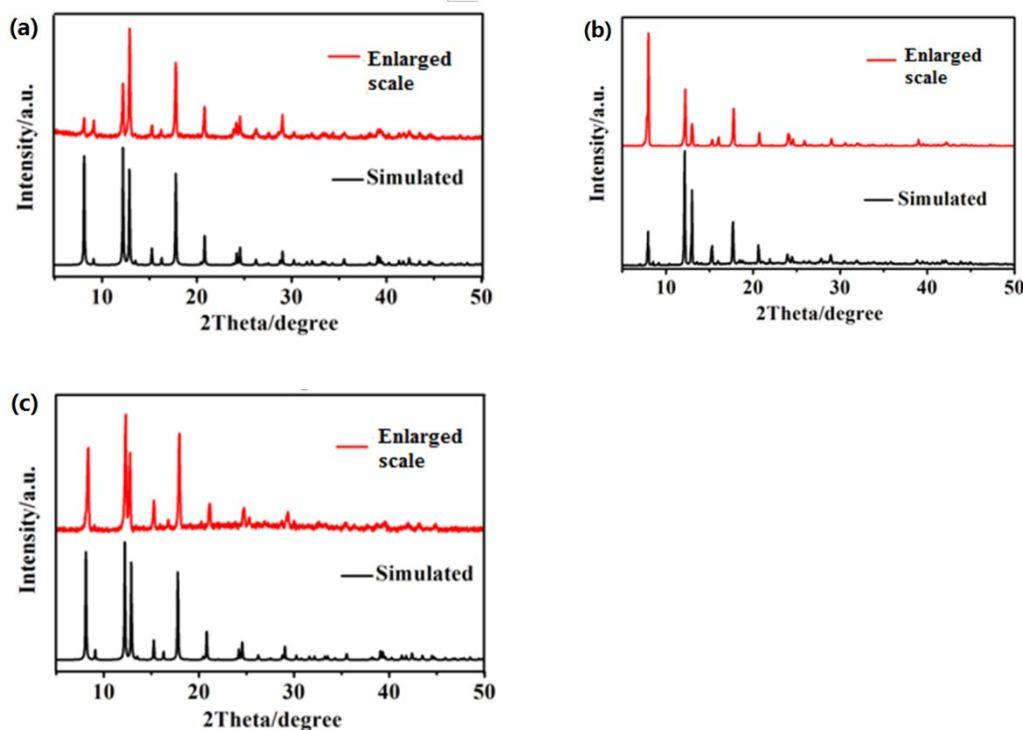
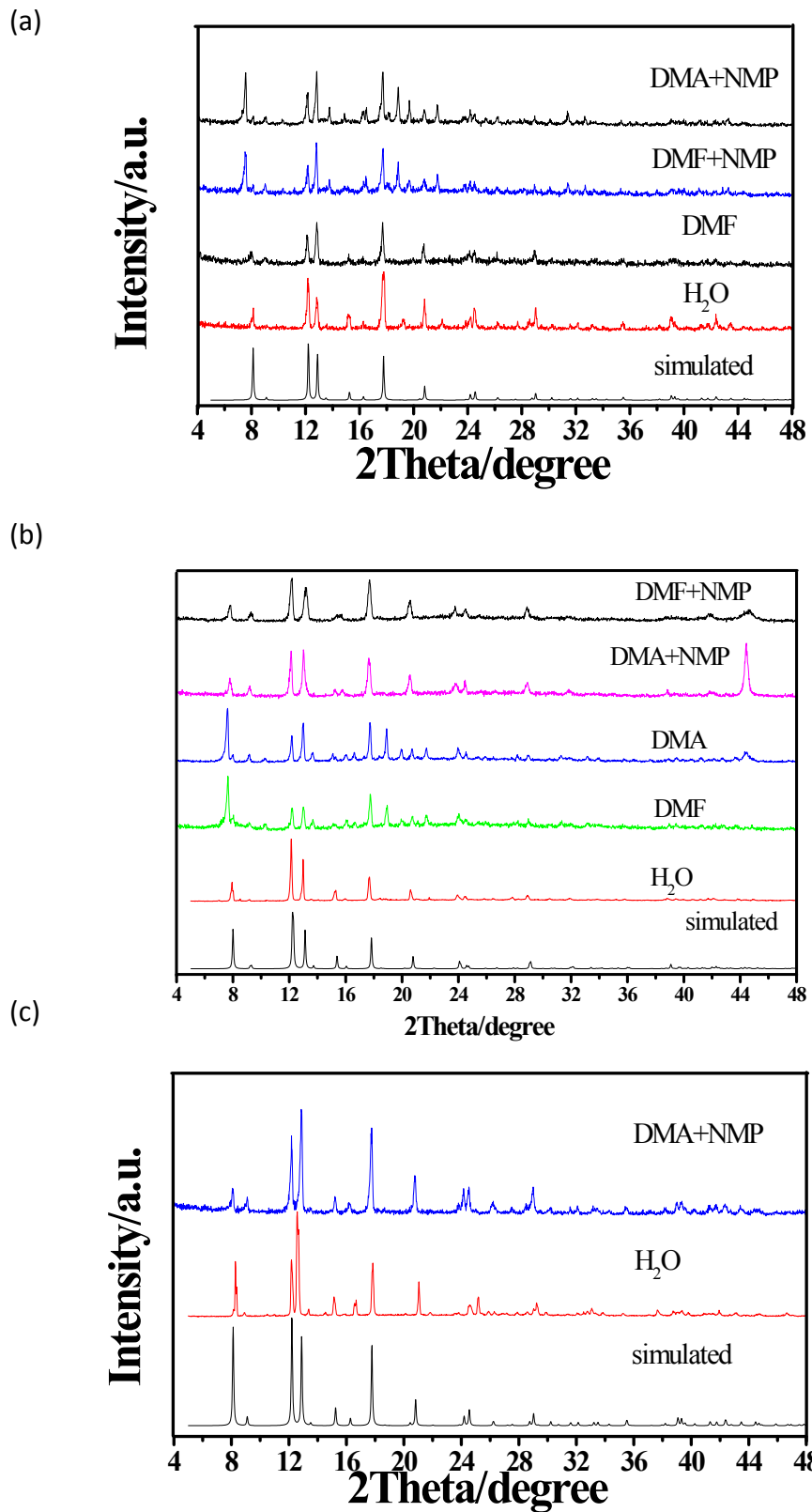


Fig. S5 The powder X-ray diffraction (PXRD) patterns of the products of large scale preparations of MOF 1(a), 2(b) and 3(c).



**Fig. S6** PXRD patterns of MOFs **1(a)**, **2(b)** and **3(c)** synthesized in various solvent systems.

**Table S2** Crystallographic data for MOFs **1-3** and **5**.

Compound	<b>1·H<sub>2</sub>O</b>	<b>2(H<sub>2</sub>O)<sub>2</sub></b>	<b>3·H<sub>2</sub>O</b>	<b>5<sup>a</sup></b>
Formula	C <sub>38</sub> H <sub>26</sub> Co <sub>2</sub> N <sub>2</sub> O <sub>9</sub> Si	C <sub>38</sub> H <sub>28</sub> Ni <sub>2</sub> N <sub>2</sub> O <sub>10</sub> Si	C <sub>38</sub> H <sub>26</sub> Cu <sub>2</sub> N <sub>2</sub> O <sub>9</sub> Si	C <sub>38</sub> H <sub>24</sub> O <sub>8</sub> N <sub>2</sub> Zn <sub>2</sub> Si
Fw	800.56	818.11	809.80	795.42
Crystal system	tetragonal	orthorhombic	tetragonal	Tetragonal
Space group	P4 <sub>2</sub> /mcm	Pccm	P4 <sub>2</sub> /mcm	P4 <sub>2</sub> /mcm
a(Å)	9.7078(3)	9.583(4)	9.7078(3)	13.9160(12)
b(Å)	9.7078(3)	9.487(3)	9.7078(3)	13.9160(12)
c(Å)	21.7592(15)	22.074(2)	21.7592(15)	21.142(4)
V(Å <sup>3</sup> )	2050.62(17)	2006.7(11)	2050.62(17)	4094.2(9)
Z	2	2	2	2
D <sub>e</sub> (g/cm <sup>3</sup> )	1.297	1.347	1.311	0.645
μ(mm <sup>-1</sup> )	0.889	1.023	1.117	0.624
T(K)	291(2)	296(2)	291(2)	100(1)
Total reflections	11473	35802	11587	29346
Unique data collected	1127	1896	1127	2287
Observed reflections	966	1671	897	2202
R <sub>int</sub>	0.0583	0.0724	0.0800	0.0466
R <sub>1</sub> , wR <sub>2</sub> (I > 2σ(I))	0.0470, 0.1628	0.0660, 0.1781	0.0471, 0.1401	0.0628, 0.1899
R <sub>1</sub> , wR <sub>2</sub> (all data)	0.0538, 0.1671	0.0769, 0.1850	0.0640, 0.1503	0.0695, 0.1944
Goodness of fit on F <sup>2</sup>	1.042	1.194	1.055	1.144

<sup>a</sup> Data is from ref. 19.

**Table S3** Selected bond distances and angles MOF **1-3**.

	<b>1</b>	<b>2<sup>a</sup></b>	<b>3<sup>a</sup></b>
Co1-N1	2.0322(39)	1.96(25)	2.0859(39)
Co1-O1	2.0189(30)	1.9992(99)	1.9824(30)
M-M	2.6354(8)	2.5554(41)	2.5801(7)
C1-O2 in <b>3</b>	-	1.276(18)	-
O1-C1	1.2474(49)	1.201(18)	1.2394(49)
C1-C2	1.5013(57)	1.51(14)	1.5142(54)
C2-C3	1.409(17)	1.397(57)	1.392(14)
C3-C4	1.360(23)	1.372(41)	1.379(19)
C4-C5	1.446(14)	1.38(20)	1.420(11)
C5-Si1	1.8743(41)	1.84 (21)	1.8940(35)
N1-C6	1.30(11)	1.37 (29)	1.283(84)
C6-C7	1.33(14)	1.408(77)	1.33(12)
C7-C8	1.405(90)	1.38(49)	1.405(88)
C12-N1 in <b>2</b>	-	1.41(29)	-
C10-C11 in <b>2</b>	-	1.3 (12)	-
C11-C12 in <b>2</b>	-	1.395(81)	-
C2-C7 in <b>2</b>	-	1.40(24)	-
C7-C8 in <b>2</b>	-	1.399(71)	-
C8-C5 in <b>2</b>	-	1.40(19)	-
O1-Co1-N1	96.043(83)	94.53(29)	95.631(84)
O1-C1-O1 <sup>ii</sup>	124.75(37)	124.8(14)	124.25(37)
C3-C2-C3 <sup>ii</sup>	111.67(89)	115(12)	109.35(70)
C6-N-C6 <sup>ii</sup>	112.5(60)	116(20)	114.3(55)
C5-Si-C5 <sup>ii</sup>	108.22(17)	102.8(77)	110.58(15)
two C1Co1Co1 planes	87.436(41)	87.67(11)	89.500(36)

<sup>a</sup> Corresponding values in MOF **2** or **3**.**Table S4** Pore sizes<sup>a</sup> (Å) and porosities<sup>b</sup> of MOFs **1-3**.

Direction	<b>1</b>	<b>2</b>	<b>3</b>
a	2.3x2.2 3.1x1.5	2.2x2.8 -	2.2x2.0 3.2x1.6..
b	as above	1.7x2.1	as above
c	1.2x1.7	0.5x0.5	1.0x1.8
a+b	1.6x3.6	1.7x2.5	1.9x3.2
Porosity <sup>b</sup>	16.3,16.9,15.5, 14.0, 14.0, 10.4	16.0,16.8,14.7, 12.9,12.6, 6.7	15.7,16.3,14.9, 14.1,13.7,8.3

<sup>a</sup>Pore sizes were determined taking into account neutral van der Waals radii of relevant atoms at the pore walls. <sup>b</sup> Porosities were measured by Platon software,<sup>20</sup> and the probing radius were 1.2 (default), 1.09 (van der Waals radius of H), 1.33 (kinetic radius of H<sub>2</sub>O), 1.52 (van der Waals radius of O, related to the size of CO<sub>2</sub>), 1.55 (van der Waals radius of N, related to the size of N<sub>2</sub>) and 1.9 (kinetic radius of CH<sub>4</sub>) and corresponding porosities are given successively.

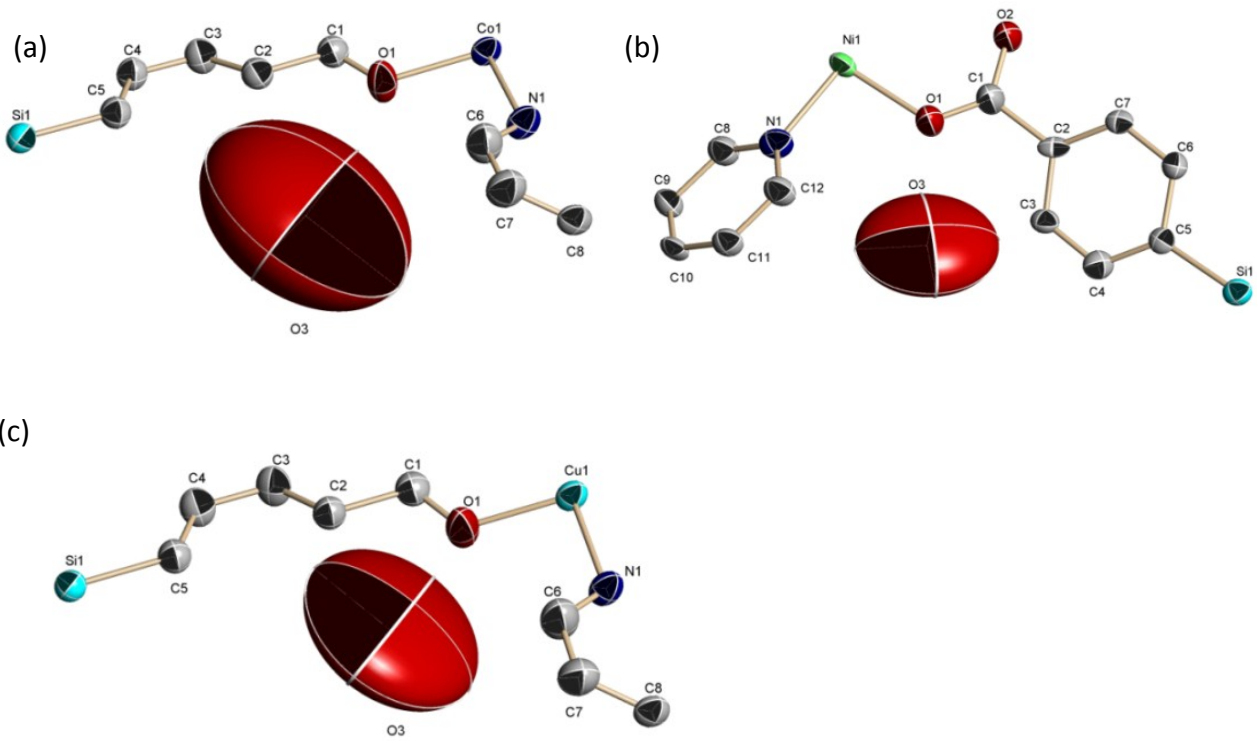


**Fig. S7** The asymmetric units of MOFs **1** (a), **2** (b) and **3** (c). Hydrogen atoms were not shown.

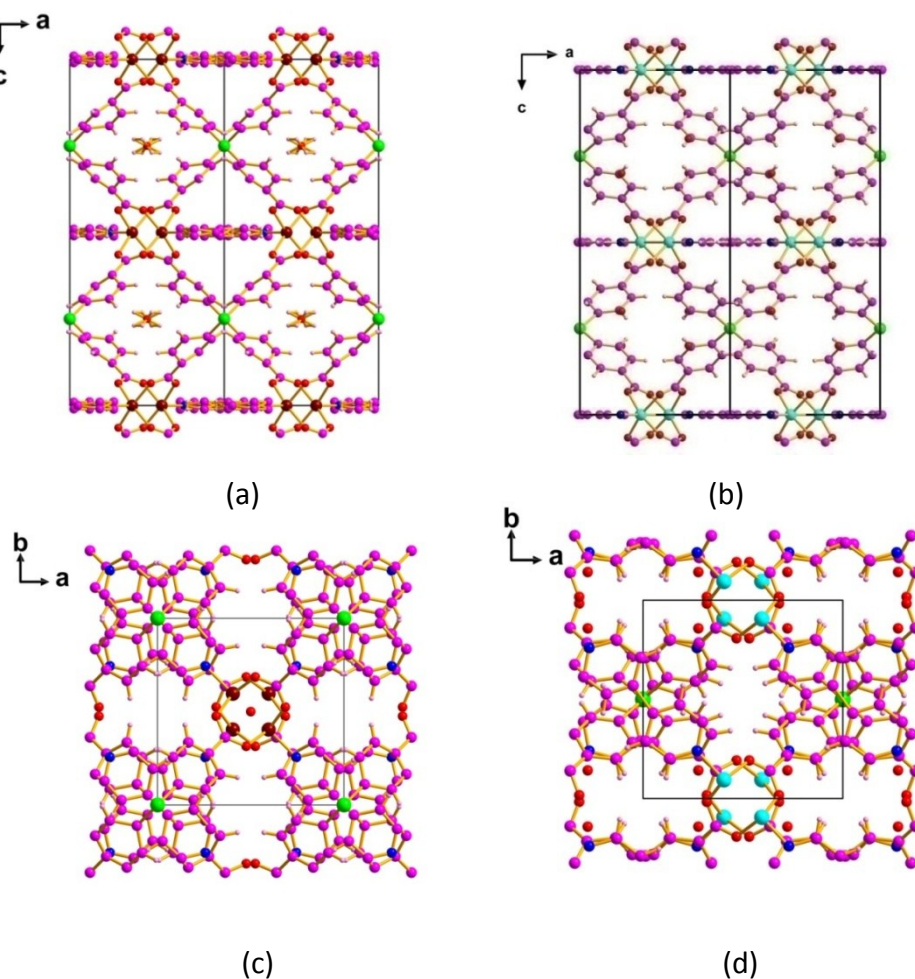


**Fig. S8** The 3D packing of MOFs **1** and **2**, viewing along *b* ((a) (**1**) and (b)(**2**)) and *c* ((c) (**1**) and (d) (**2**)) axes.

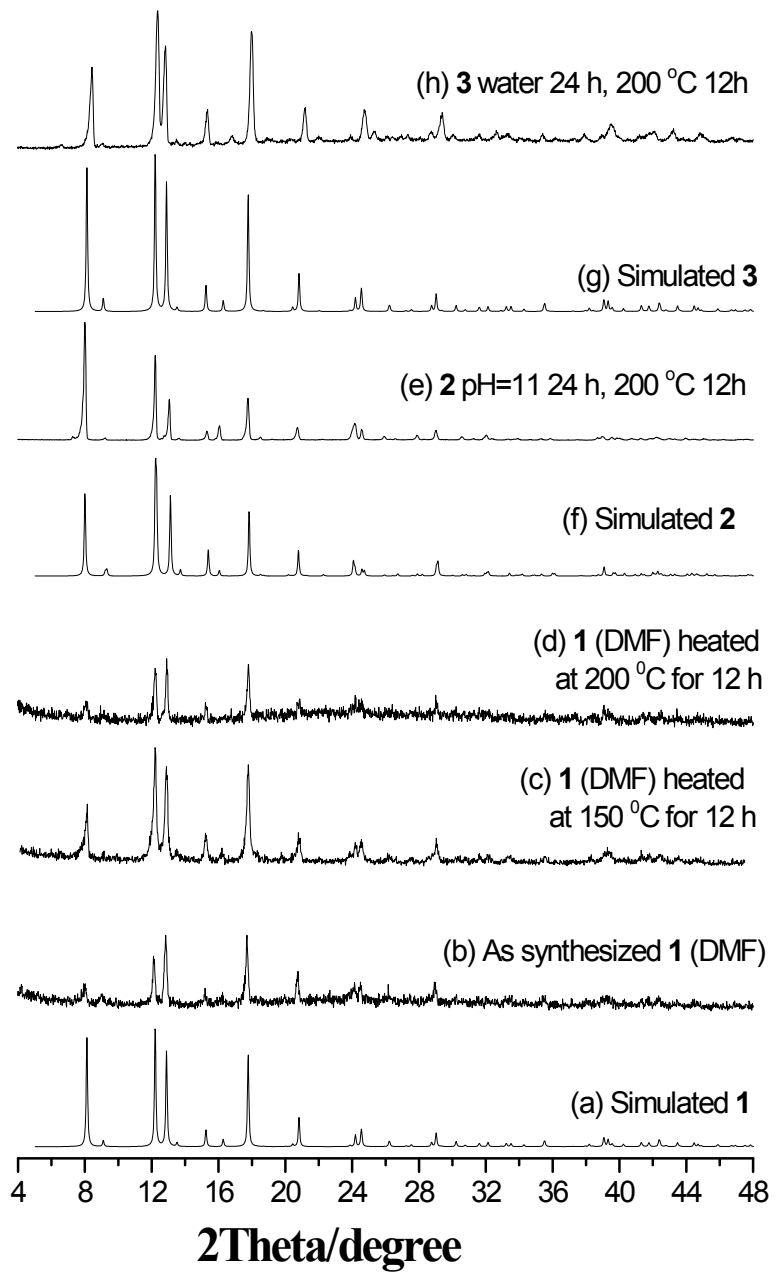


**Fig. S9** PXRD of MOFs **1-3** heated at various temperatures for 12 h.

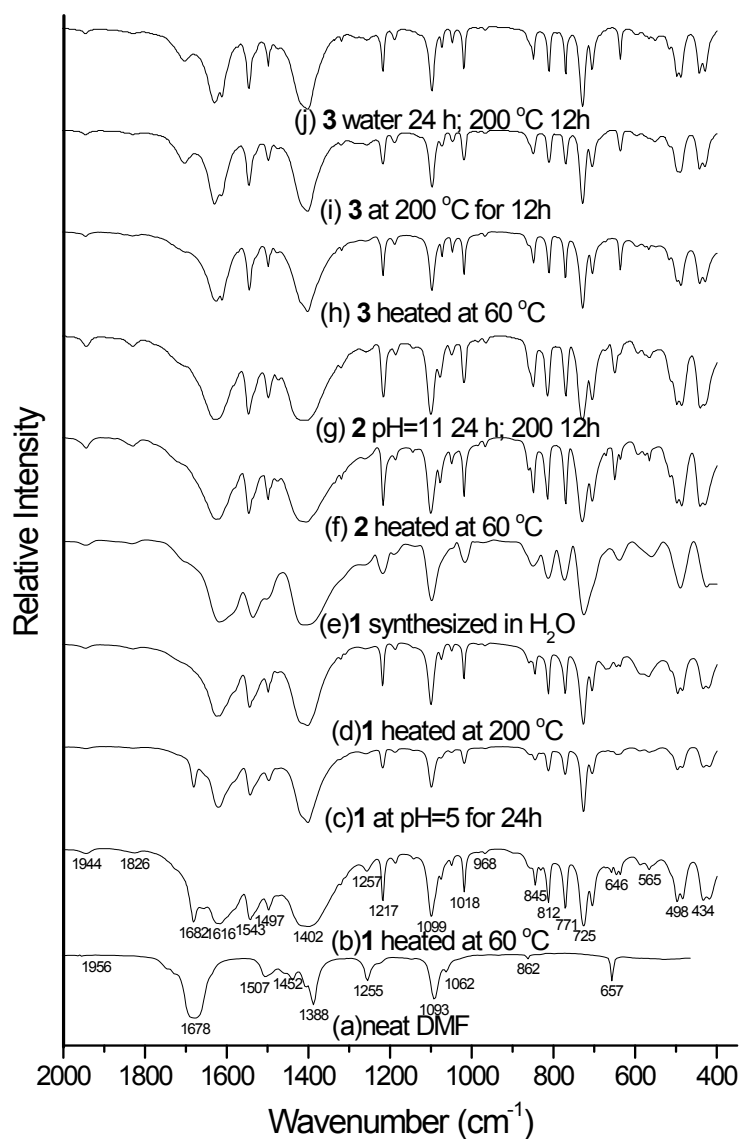


**Fig. S10** Thermal stability of MOFs **1- 3** checked by IR spectra.

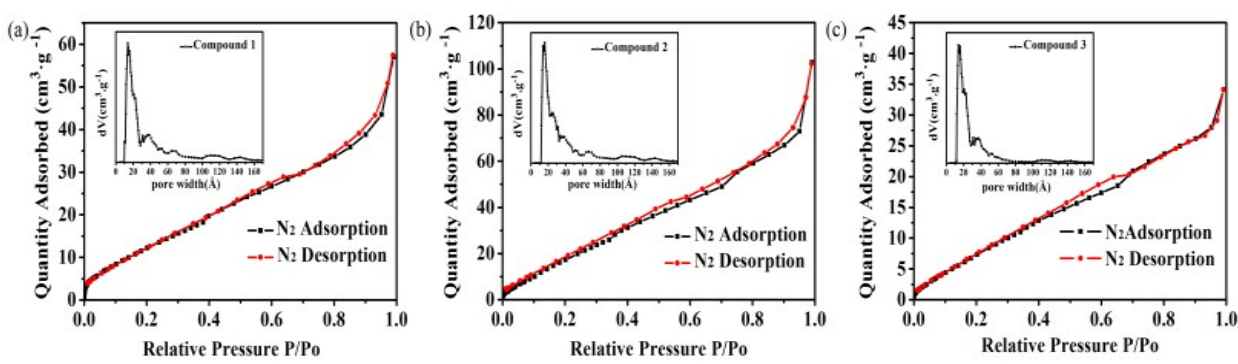


**Fig. S11** Nitrogen gas sorption isotherms for MOFs **1** (a) , **2** (b) and **3** (c) measured at 77 K (black and red symbols represent adsorption and desorption data, respectively). Insets: Pore size distribution.

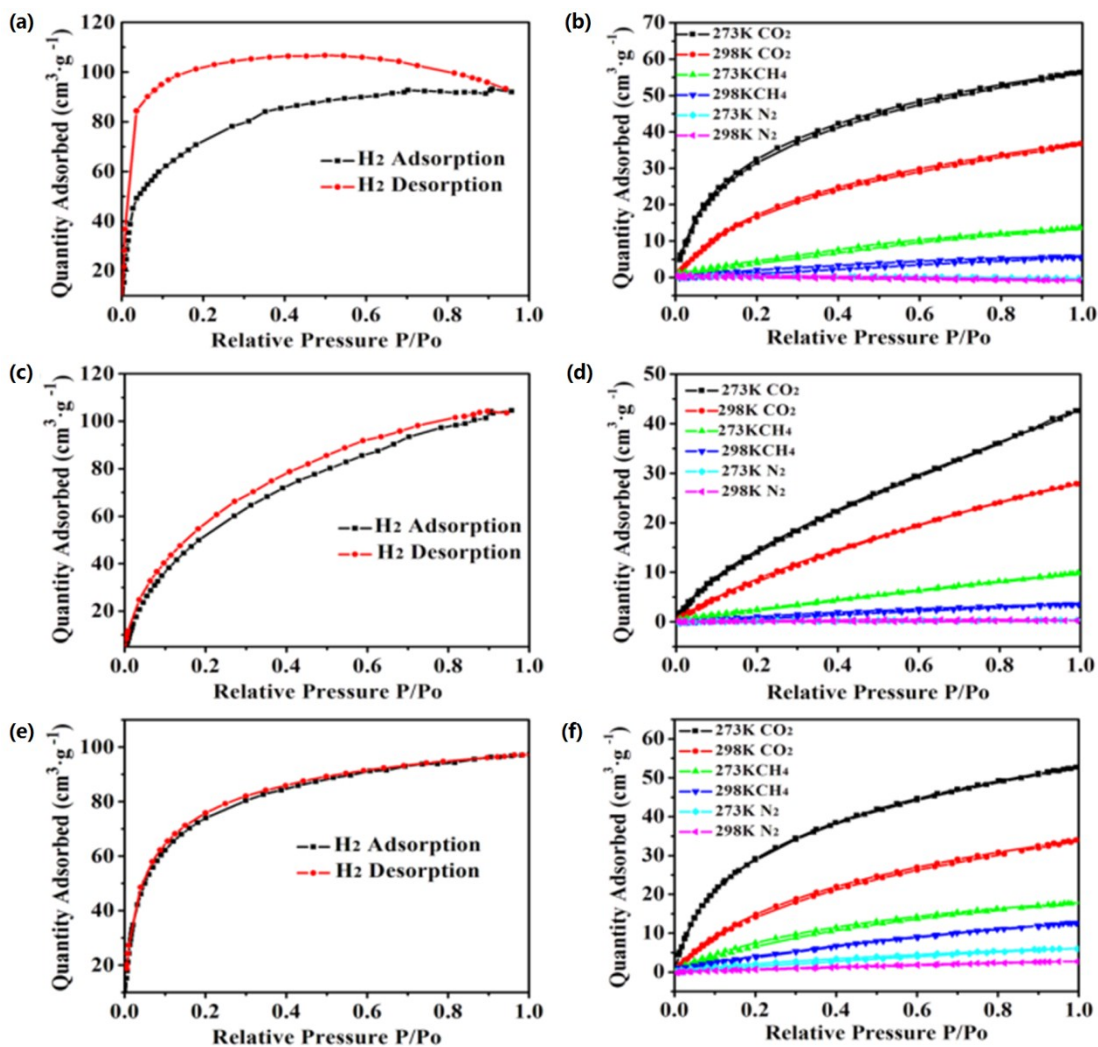


**Fig. S12** The H<sub>2</sub> sorption isotherms for MOFs **1** (a), **2** (c) and **3** (e) measured at 77 K (black and red symbols represent adsorption and desorption data, respectively); The N<sub>2</sub>, CH<sub>4</sub> and CO<sub>2</sub> sorption isotherms for MOFs **1**(b), **2**(d) and **3**(f) measured at 298 and 273 K.

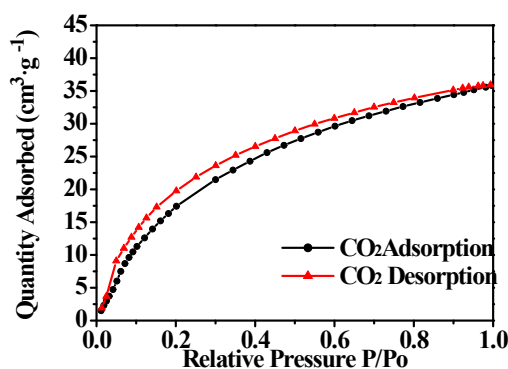


**Fig. S13** CO<sub>2</sub> sorption isotherms of compound **3** (recovered after 24 h in water) at 298 K.

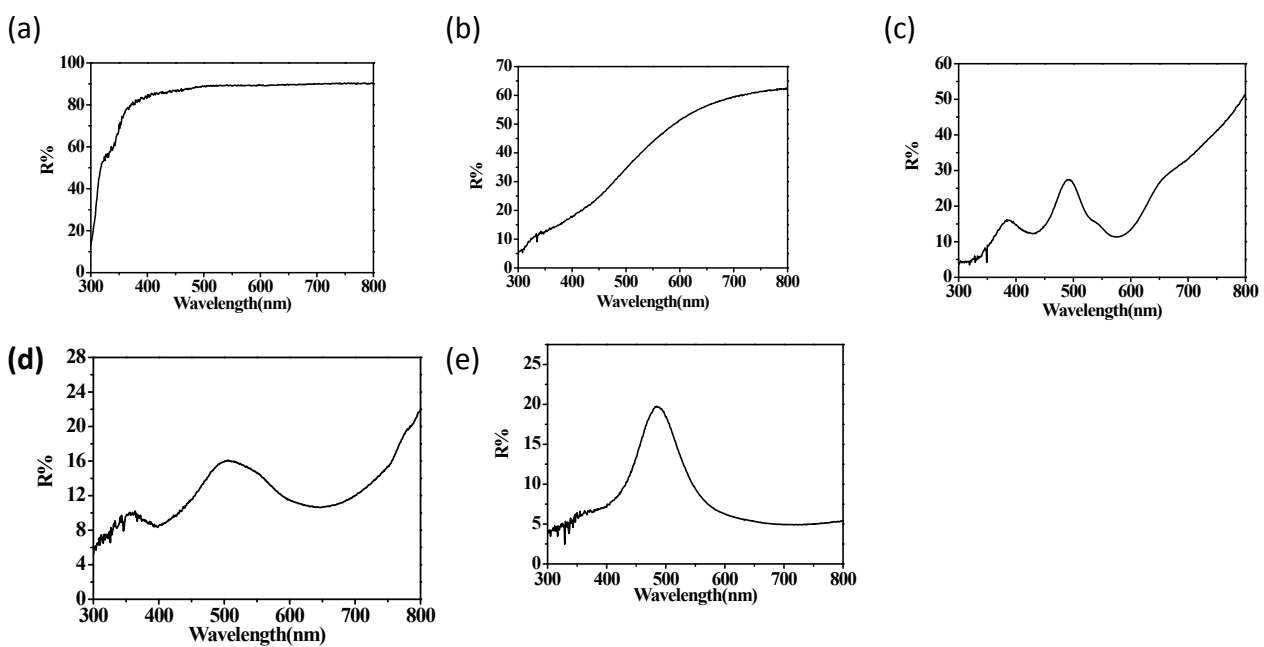


**Fig. S14** UV-Vis spectra (R% versus Wavelength) of H<sub>4</sub>TCS (a), BPY (b) MOF 1 (c), 2 (d) and 3 (e).

**Table S5** The total energies of the optimized structures of the unit cells of MOFs 1-3 using the GGA-PBE method.

MOFs	Type of Materials	Energy (eV)	Engery Difference (eV)
1	Paramagnetic	$E_1 = -1044.0760$	$E_1-E_2 = 0.0001$
	Antiferromagnetic	$E_2 = -1044.0761$	$E_2-E_2 = 0$
	Ferromagnetic	$E_3 = -1044.0761$	$E_3-E_2 = 0$
2	Paramagnetic	$E_1 = -1036.0028$	$E_1-E_3 = 0.7794$
	Antiferromagnetic	$E_2 = -1036.0096$	$E_2-E_3 = 0.7726$
	Ferromagnetic	$E_3 = -1036.7822$	$E_3-E_3 = 0$
3	Paramagnetic	$E_1 = -1027.0966$	$E_1-E_2 = 0.2379$
	Antiferromagnetic	$E_2 = -1027.3345$	$E_2-E_2 = 0$
	Ferromagnetic	$E_3 = -1027.0978$	$E_3-E_2 = 0.2467$

**Table S6** Valence and conduction band edges and band gaps of MOF 1 and 3 calculated by GGA-PBE and different GGA-PBE + U methods.<sup>a</sup>

MOF	Method	Spin-up electrons	Method	Spin-up electrons
1	PBE	$V_{MAX} = -0.696$	U=4.0 J=1.0	$V_{MAX} = -0.881$
		$C_{MIN} = 0.577$		$C_{MIN} = 0.857$
		$E_g = 1.27$		$E_g = 1.74$
	U=3.3	$V_{MAX} = -0.875$	U=5.0 J=1.0	$V_{MAX} = -0.867$
		$C_{MIN} = -0.854$		$C_{MIN} = -0.8465$
		$E_g = 1.73$		$E_g = 1.71$
	U=4.0	$V_{MAX} = -0.867$		
		$C_{MIN} = 0.846$		
		$E_g = 1.71$		
3	PBE	$V_{MAX} = -0.131$	U=4.0	$V_{MAX} = -0.200$
		$C_{MIN} = 0.188$		$C_{MIN} = 0.198$
		$E_g = 0.32$		$E_g = 0.40$
	U=3.0	$V_{MAX} = -0.202$	U=5.0	$V_{MAX} = -0.201$
		$C_{MIN} = 0.192$		$C_{MIN} = 0.200$
		$E_g = 0.39$		$E_g = 0.40$
	U=3.3	$V_{MAX} = -0.199$	U=4.0 J=1.0	$V_{MAX} = -0.204$
		$C_{MIN} = 0.196$		$C_{MIN} = 0.190$
		$E_g = 0.40$		$E_g = 0.39$

<sup>a</sup>  $V_{max}$  represents the maximum of the valence band edge,  $C_{min}$  represents the minimum of the conduction band edge. Since the band structures of the spin-down electrons of 1 and 3 are the same as those of the spin-up electrons, only the information on the spin-up electrons are given.

**Table S7** Valence and conduction band edges and band gaps of MOF **2** calculated by GGA-PBE and different GGA-PBE + U methods.

<sup>a</sup>

Method	Spin-up electrons	Spin-down electrons	$E_g'$ <sup>b</sup>
PBE	$V_{MAX} = -0.080$	$V_{MAX} = -0.642$	1.04
	$C_{MIN} = 0.956$	$C_{MIN} = 0.956$	
	$E_g = 1.04$	$E_g = 1.60$	
U=3.0	$V_{MAX} = -0.223$	$V_{MAX} = -0.275$	0.42
	$C_{MIN} = 1.636$	$C_{MIN} = 0.197$	
	$E_g = 1.86$	$E_g = 0.47$	
U=3.3	$V_{MAX} = -1.130$	$V_{MAX} = -0.300$	0.59
	$C_{MIN} = 0.292$	$C_{MIN} = 1.594$	
	$E_g = 1.42$	$E_g = 1.89$	
U=4.0	$V_{MAX} = -0.329$	$V_{MAX} = -0.178$	0.36
	$C_{MIN} = 0.180$	$C_{MIN} = 1.680$	
	$E_g = 0.51$	$E_g = 1.86$	
U=6.4	$V_{MAX} = -0.964$	$V_{MAX} = -1.619$	1.92
	$C_{MIN} = 1.538$	$C_{MIN} = 0.955$	
	$E_g = 2.50$	$E_g = 2.57$	

<sup>a</sup>  $V_{max}$  represents the maximum of the valence band edge,  $C_{min}$  represents the minimum of the conduction band edge. <sup>b</sup>  $E_g'$  is the difference between the valence band edge and the conduction band edge of all the electrons.

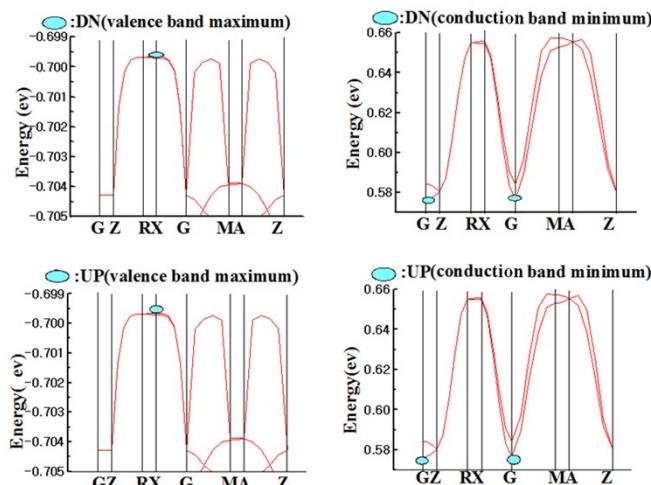


**Fig. S15** Enlarged band structures (GGA-PBE method) of the spin-up and spin-down electrons of MOF **1**, showing MOF **1** is an indirect band gap semiconductor.

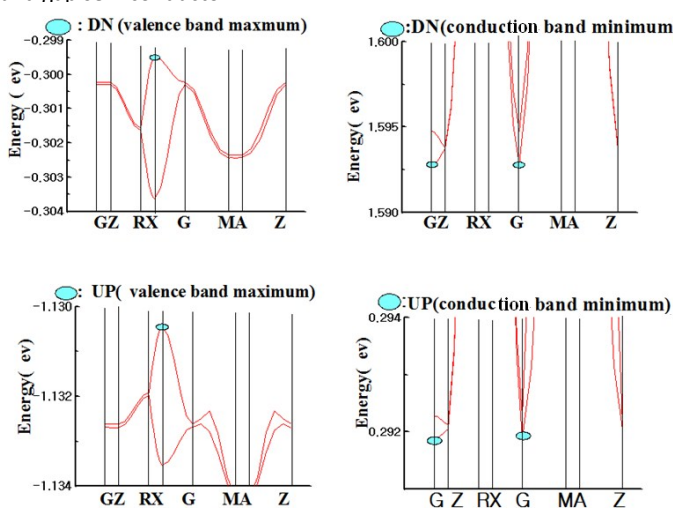


**Fig. S16** Enlarged band structures (GGA-PBE + U ( $U=3.3$ ) method) of the spin-up and spin-down electrons of MOF **2**, showing it is an indirect band gap semiconductor.

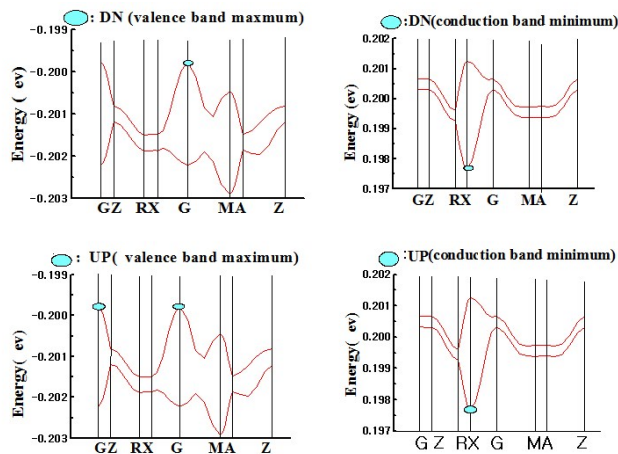


**Fig. S17** Enlarged band structures (GGA-PBE + U ( $U = 4.0$ ) method) of the spin-up and spin-down electrons of MOF **3**, showing it is an indirect band gap semiconductor.

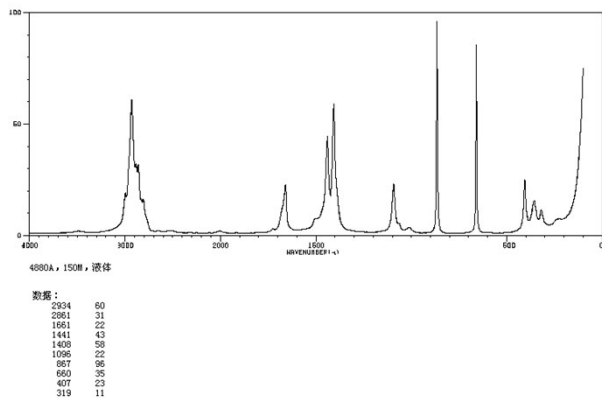


**Fig. S18** Raman Spectrum of the liquid N,N-dimethylformamide (from [http://www.basechem.org/\\_chemical/image/20#](http://www.basechem.org/_chemical/image/20#))

## References

- 1 T.-F. Yeh, S.-J. Chen, C.-S. Yeh and H. Teng, *J. Phys. Chem. C*, 2013, **117**, 6516-6524.
- 2 G.-L. Wang, J.-X. Shu, Y.-M. Dong, X.-M. Wu, W.-W. Zhao, J.-J. Xu and H.-Y. Chen, *Anal. Chem.*, 2015, **87**, 2892-2900.
- 3 X. Shi, H. Wang, Y. Li, J. Yang, L. Chen, G. Hui, W. Xu and B. Zhao, *Chem. Res. Chin. Univ.*, 2010, **26**, 1011-1015.
- 4 A. Topaçlı and S. Akyüz, *Spectroc. Acta Pt. A-Molec. Biomolec. Spectr.*, 1995, **51**, 633-641.
- 5 B. Zhang and Z. Wang, *Chem. Mater.*, 2010, **22**, 2780-2789.
- 6 N. R. Dhumal, M. P. Singh, J. A. Anderson, J. Kiefer and H. J. Kim, *J. Phys. Chem. C*, 2016, **120**, 3295-3304.
- 7 C. Prestipino, L. Regli, J. G. Vitillo, F. Bonino, A. Damin, C. Lamberti, A. Zecchina, P. L. Solari, K. O. Kongshaug and S. Bordiga, *Chem. Mater.*, 2006, **18**, 1337-1346.
- 8 J. B. DeCoste, G. W. Peterson, B. J. Schindler, K. L. Killops, M. A. Browne and J. J. Mahle, *J. Mater. Chem. A*, 2013, **1**, 11922-11932.
- 9 M. W. Zhang, Y. P. Chen and H. C. Zhou, *Crystengcomm*, 2013, **15**, 9544-9552.
- 10 K. Tan, N. Nijem, P. Canepa, Q. Gong, J. Li, T. Thonhauser and Y. J. Chabal, *Chem. Mater.*, 2012, **24**, 3153-3167.
- 11 E. Pretsch, P. Buhlmann and M. Badertscher, *Structure Determination of Organic Compounds*, Springer Berlin Heidelberg, 2009.
- 12 G. B. Deacon and R. J. Phillips, *Coord. Chem. Rev.*, 1980, **33**, 227-250.
- 13 V. Zeleňák, Z. Vargová and K. Györyová, *Spectroc. Acta Pt. A-Molec. Biomolec. Spectr.*, 2007, **66**, 262-272.
- 14 K. Helios, R. Wysokinski, A. Pietraszko and D. Michalska, *Vib. Spectrosc.*, 2011, **55**, 207-215.
- 15 K. Nakamoto, *Infrared and Raman Spectra of Inorganic and Coordination Compounds*, John Wiley & Sons, Inc., Hoboken, New Jersey, 2009.
- 16 P. Drozdzewski and B. Pawlak, *Vib. Spectrosc.*, 2003, **33**, 15-20.
- 17 M. K. Bhunia, J. T. Hughes, J. C. Fettinger and A. Navrotsky, *Langmuir*, 2013, **29**, 8140-8145.
- 18 N. Drenchev, E. Ivanova, M. Mihaylov and K. Hadjiivanov, *Phys. Chem. Chem. Phys.*, 2010, **12**, 6423-6427.
- 19 J. J. Wang, J. Zhang, F. Y. Jin, Y. P. Luo, S. F. Wang, Z. Y. Zhang, Y. Wu, H. K. Liu, J. Y. Luc and M. Fang, *Crystengcomm*, 2015, **17**, 5906-5910.
- 20 A. L. Spek, *J. Appl. Cryst.*, 2003, **36**, 7-13.